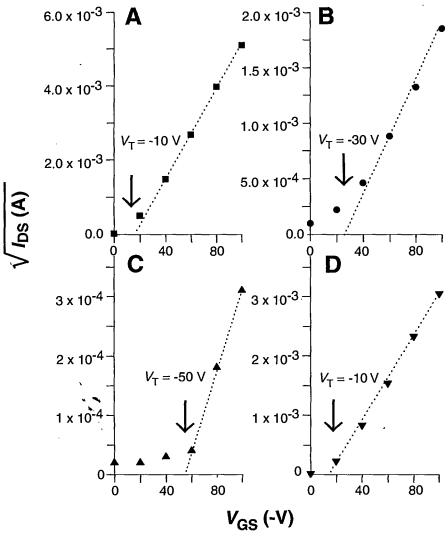

Fig. 4. Plots of $(I_{DS})^{1/2}$ versus V_{GS} for an α-6T TFT (L = 12 μm, V_{DS} = −100 V) at different temperatures: (**A**) T = 300 K; (**B**) T = 100 K; (**C**) T = 45 K; and (**D**) T = 3.8 K. The intercepts of the dotted straight lines with the V_{GS} axis give the device threshold voltage (V_T), and the slopes are proportional to μ_{FET}.

independent sets of experimental evidence that show that grain boundaries do not act as the mobility-limiting mechanisms (for $n > n_T$). In (*23*) we showed that the room-temperature mobility in α-6T TFTs does not improve when the crystalline grains are enlarged by an order of magnitude and the grain boundaries greatly decrease in extent.

The second piece of evidence, which also indicates that grain boundaries do not dominate transport, can be obtained from the data of Fig. 4, A through D, which indicate that for $n > n_T$, the square root of I_{DS} at different temperatures increases linearly with V_{GS} (proportional to n). Particularly interesting is the T = 3.8 K case (Fig. 4D). The constant mobility in the "delocalized" regime, which occurs only within each crystallite, implies that the grain boundaries are not the mobility-limiting mechanisms. Trap filling neutralizes the effect of traps on the transport above T_T, so that intrinsic activated hopping behavior between α-6T molecules can be observed. In fact, there is always a linear relation between induced carried density and V_{GS} beyond the threshold voltage. The surface states at the gate dielectric–active material interface also do not play a substantial role; similar behavior of μ_{FET} versus T was found in a sample where the gate dielectric material was changed from SiO_2 to MgF_2 (*24*).

We conclude that grain boundaries, traps, and surface states (for charge densities $n > n_T$ and $T > T_T$) do not substantially influence the mobility in high-quality samples. We can thus extract values for J, γ, and ω_0 that predict room-temperature mobilities for α-6T of ~0.02 $cm^2\ V^{-1}\ s^{-1}$, which is consistent with our highest measured room-temperature mobility (without high electric field effects), which is 0.02 to 0.03 $cm^2\ V^{-1}\ s^{-1}$ (*25*). This result suggests that our TFTs already exhibit μ_{FET} close to the highest achievable μ_{FET} at 300 K, according to Holstein's formalism. Because, within this picture, the hopping mobility μ is proportional to $\exp(-E_B)$ (*7*), we can enhance μ by choosing materials with lower polaron binding energy or low carrier-lattice coupling.

REFERENCES AND NOTES

1. F. Garnier, R. Hajlaoui, A. Yassar, P. Srivastava, *Science* **265**, 1684 (1994).
2. A. Dodabalapur, L. Torsi, H. E. Katz, *ibid.* **268**, 270 (1995).
3. A. Dodabalapur, H. E. Katz, L. Torsi, R. C. Haddon, *ibid.* **269**, 1560 (1995).
4. A. J. Lovinger *et al.*, *J. Mater. Res.* **10**, 2958 (1995).
5. G. Horowitz, R. Hajlaoui, P. Delannoy, *J. Phys. III Fr.* **5**, 355 (1995); K. Wargai *et al.*, *Phys. Rev. B* **52**, 1786 (1995).
6. J. Ostrick *et al.*, unpublished results.
7. T. Holstein, *Ann. Phys.* **8**, 343 (1959).
8. N. F. Mott, *Metal-Insulator Transitions* (Taylor and Francis, London, 1990), pp. 59–68.
9. R. F. Kiefl *et al.*, *Phys. Rev. Lett.* **62**, 792 (1989).
10. L. Torsi, A. Dodabalapur, H. E. Katz, *J. Appl. Phys.* **78**, 1088 (1995).
11. H. E. Katz, A. Dodabalapur, L. Torsi, D. Elder, *Chem. Mater.* **7**, 2238 (1995).
12. S. M. Sze, *Physics of Semiconductor Devices* (Wiley, New York, 1981).
13. S. Kojima, *Phys. Rev. B* **47**, 2924 (1993).
14. E. M. Conwell, H. Y. Choi, S. Jeyadev, *J. Phys. Chem.* **96**, 2827 (1992).
15. Along the transport direction, α-6T has a herringbone-type molecular arrangement. The crystal structure is described in (*4*) and in T. Siegrist *et al.* [*J. Mater. Res.* **10**, 2173 (1995)]. We take for the intermolecular spacing the nearest distance between adjacent molecules, which is ~3.8 Å.
16. M. G. Harrison, R. H. Friend, F. Garnier, A. Yassar, *Synth. Metals* **67**, 215 (1994).
17. I. G. Austin. *J. Phys. C* **5**, 1687 (1972).
18. Yu. A. Firsov, *Semiconductors* **29**, 515 (1995).
19. Some early batches of α-6T were dominated by extrinsic effects, and therefore the mobility at $T < T_T$ was too low to permit an observer to see the transition.
20. A. L. Shluger and A. M. Stoneham, *J. Phys. Condens. Matter.* **5**, 3049 (1993).
21. J. M. G. Cowie, *Polymers: Chemistry and Physics of Modern Materials* (Chapman and Hall, New York, 1991), pp. 256–257; S. Matsuoka, *Relaxation Phenomena in Polymers* (Hanser, New York, 1992), p. 224.
22. W. Warta and N. Karl, *Phys Rev B* **A32**, 1172 (1985).
23. L. Torsi *et al.*, *Chem. Mater.* **7**, 2247 (1995).
24. The transistors that have a MgF_2 gate dielectric also show all the features that transistors with a SiO_2 gate do.
25. It may be possible (but unlikely) that we are consistently underestimating μ_{FET} as a result of imperfect ohmic contacts. If this is the case, the data points and the calculated mobilities in Fig. 2 will be offset along the y axis.

26. We thank F. Capasso, E. A. Chandross, R. C. Haddon, P. B. Littlewood, A. J. Lovinger, A. P. Mills, J. C. Phillips, E. Reichmanis, G. Scamarcio, T. Siegrist, and R. E. Slusher for their encouragement and illuminating discussions.

30 January 1996; accepted 3 April 1996

Lithospheric Contributions to Arc Magmatism: Isotope Variations Along Strike in Volcanoes of Honshu, Japan

Annie B. Kersting,* Richard J. Arculus, David A. Gust

Major chemical exchange between the crust and mantle occurs in subduction zone environments, profoundly affecting the chemical evolution of Earth. The relative contributions of the subducting slab, mantle wedge, and arc lithosphere to the generation of island arc magmas, and ultimately new continental crust, are controversial. Isotopic data for lavas from a transect of volcanoes in a single arc segment of northern Honshu, Japan, have distinct variations coincident with changes in crustal lithology. These data imply that the relatively thin crustal lithosphere is an active geochemical filter for all traversing magmas and is responsible for significant modification of primary mantle melts.

Unraveling the extent to which arc magmas are modified during ascent is a prerequisite for understanding the primary petrologic characteristics of their sources and the petrogenetic processes involved in magma generation. Isotopic data in combination with the chemical composition of arc lavas are crucial for tracing potential source contributions to these magmas (*1*). The major magma source in island arcs is the peridotitic mantle wedge, fluxed by subducted, slab-derived fluids (*2*). An additional contribution may come during magma passage through overriding lithosphere. For example, in the southern Andes, geochemical differences in andesite-rhyolite suites reflect increased crustal contributions to magma genesis coincident with an approximate doubling in crustal thickness to >70 km (*3*). Other

A. B. Kersting, Earth Science Division and Institute of Geophysics and Planetary Physics, Lawrence Livermore National Laboratory, L-231, Post Office Box 808, Livermore, CA 94551, USA.
R. J. Arculus, Key Centre for the Geochemical Evolution and Metallogeny of Continents, Department of Geology, Australian National University, Canberra, ACT 0200, Australia.
D. A. Gust, School of Geology, Queensland University of Technology, Brisbane, QLD 4001, Australia.
*To whom correspondence should be addressed.

studies have shown the importance of crustal processes in the production of evolved, high-SiO_2 lavas (3–5), yet the impact of the lithosphere with a thin crust on less evolved, basaltic magmas is uncertain (6).

To evaluate the contribution of the lithosphere to arc evolution, we examined a transect of ten, along-strike Quaternary volcanoes in northern Honshu, Japan, where less evolved basaltic lavas have erupted through a relatively thin crust of constant thickness. This transect of mature, compound, stratovolcanoes crosscuts a tectonic boundary where two distinct crustal terranes are juxtaposed (Fig. 1). The age of the subducting Pacific Plate (130×10^6 years old) (7), inbound sediment thickness (800 m) (8), depth to the Wadati-Benioff Zone (WBZ) (~100 km) (9), distance to the trench axis (250 to 300 km) (9), and crustal thickness (30 km) (9) are constant along the transect, minimizing the potential variability of these parameters to the chemistry of the rocks. The close proximity of the volcanoes (<250 km) on a single arc segment and constant depth to the WBZ also minimizes potential chemical and thermal variability in the mantle wedge. The thickness of the Honshu crust is constant; thus, variation in melting systematics along strike should be minimized (*10*). The relative contributions from the mantle wedge and subducting slab to the Honshu lavas should be constant over the arc segment investigated, leaving the juxtaposition of distinctive crustal lithospheres the remaining petrogenetic variable.

The two terranes are separated by the Tanakura tectonic line (TTL) (Fig. 1), a fundamental Mesozoic terrane boundary in northern Honshu (*11*) that was reactivated as a lithosphere-penetrating, transcurrent fault during the Oligocene-Miocene opening of the Japan Sea (*12*). Volcanoes south of the TTL overlie the Ashio terrane, which is part of the Tamba-Mino-Ashio terrane that forms the central part of southwest Honshu (*11*) and that was welded to Asia earlier than the Jurassic (*13*). Volcanoes north of the TTL overlie the Abukuma massif, once part of a microcontinent that collided with Asia during the Early Cretaceous (*13*). Crustal granitoids are younger (~60×10^6 to 100×10^6 years old) and more radiogenic in $^{87}Sr/^{86}Sr$ (~0.708 to 0.710) south of the TTL than to the north (100×10^6 to 110×10^6 years old; <0.706) (*14*).

Although the most felsic lavas erupted exclusively south of the TTL, relatively primitive basalts (>5% by weight MgO) erupted both north and south of the TTL (Fig. 2A). At a given SiO_2 content, used as a proxy for fractionation index, there is extensive overlap in K_2O abundances for volcanic rocks north and south of the TTL (Fig. 2B) and generally no consistent difference in major or trace element (for example, Pb and Sr; Fig. 2, C and D) abundances. Both suites are characterized by ratios of high alkali and alkaline-earth elements to high-field-strength elements typical of arc magmas.

The radiogenic isotopes of Pb, Sr, and

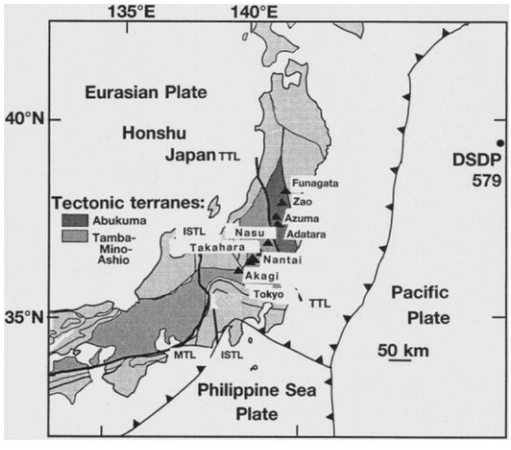

Fig. 1. Simplified tectonic map of northern Honshu, Japan, showing the locations of the volcanoes (triangles) investigated in this study [after Ichikawa (*25*)]. Three volcanoes—Nantai, Nyoho, and Nikko Shirani—form a volcanic group designated as Nantai. The TTL, ISTL (Itoigawa Shizuoka tectonic line), and MTL (median tectonic line) are major fault boundaries shown by heavy lines. South of the TTL, the Ashio terrane is a Late Paleozoic–Mesozoic sedimentary complex consisting of Permian to Middle Jurassic olistostromes and has been correlated with the Nadanhata terrane on the Asian continent (*11*). The Abukuma terrane is a younger terrane (estimated as Early Jurassic to Late Cretaceous) consisting in part of a granitic-metamorphic complex (*26*).

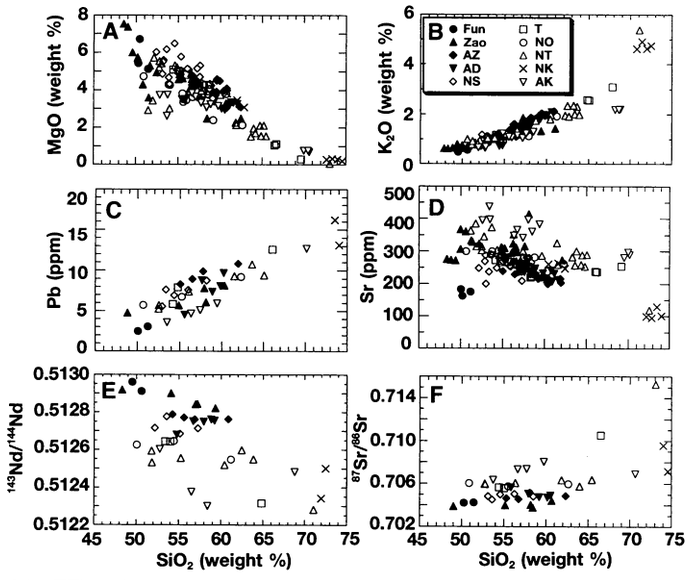

Fig. 2. Whole-rock data [by x-ray fluorescence except Pb by inductively coupled plasma-mass spectrometry (ICP-MS)] for selected major oxides and trace elements versus SiO_2: (**A**) MgO content; (**B**) K_2O content; (**C**) Pb content; (**D**) Sr content; (**E**) $^{143}Nd/^{144}Nd$; (**F**) $^{87}Sr/^{86}Sr$. Each symbol [shown in (B) and used throughout] represents a different volcano: Fun = Funagata, Zao = Zao, AZ = Azuma, AD = Adatara, NS = Nasu, T = Takahara, NO = Nyoho, NT = Nantai, NK = Nikko Shirane, and AK = Akagi; north of the TTL is designated by filled symbols; south of the TTL, by open symbols.

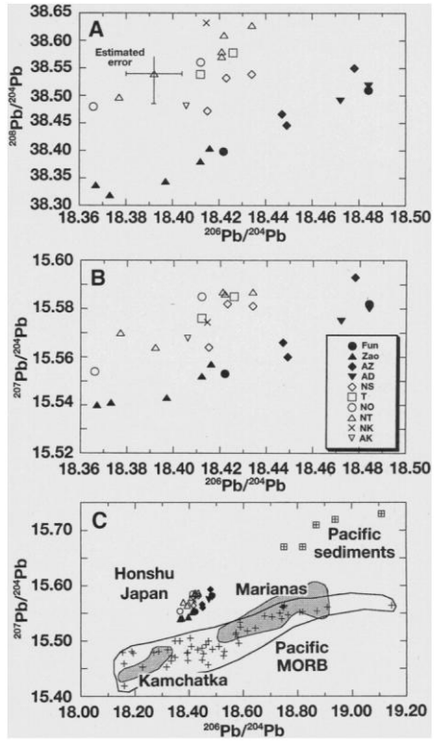

Fig. 3. (**A** and **B**) Plots of $^{208}Pb/^{204}Pb$ and $^{207}Pb/^{204}Pb$ ratios versus $^{206}Pb/^{204}Pb$ ratios of the Honshu lavas. (**C**) Honshu data compared to the data for Pacific MORB (*27*) and Pacific sediments from DSDP leg 86, hole 579, located east of the Japan trench (*20*) (see Fig. 1). Data from the Marianas (*28*) and Kamchatka (*29*) arcs are shown for comparison.

Nd show distinct systematic differences between the two volcanic suites (Table 1). For example, the $^{208}Pb/^{204}Pb$ and $^{207}Pb/^{204}Pb$ ratios at a given $^{206}Pb/^{204}Pb$ and the $^{87}Sr/^{86}Sr$ ratio are higher in lavas to the south than in those to the north of the TTL, whereas the converse is true of $^{143}Nd/^{144}Nd$ (Fig. 3, A and B; Fig. 4A). All lavas have significantly elevated $^{208}Pb/^{204}Pb$ and $^{207}Pb/^{204}Pb$ ratios compared to typical depleted mantle values [Pacific mid-ocean ridge basalt (MORB) values in Fig. 3C], and the entire Honshu transect has much lower $^{143}Nd/^{144}Nd$ and elevated $^{87}Sr/^{86}Sr$ ratios by comparison with MORB values (Fig. 4A). The Honshu data are also significantly different from data for other arcs, such as Marianas and Kuriles-Kamchatka (Figs. 3C and 4A). Even the least fractionated, most primitive lavas have Pb, Sr, and Nd isotopic ratios significantly different from those of MORBs. The distinct differences in the Pb, Sr, and Nd isotopic ratios persist when lavas of the two suites at similar levels of chemical evolution are compared (Fig. 2, E and F).

The only exception to the clear isotopic separation between the two volcanic groups is Nasu volcano, located immediately south of the TTL. The Pb isotopic ratios for Nasu volcano are intermediate between those of the north and south volcanic groups, whereas the Sr and Nd isotopic ratios overlap with data from a volcano immediately north of the TTL (Adatara). We speculate that entrainment of "northern-type" beneath "southern-type" crust south of the TTL may have occurred either because of the dip of the TTL or during the accretion of Abukuma terrane along the eastern margin of Asia.

The origins of the distinctive isotopic signatures of the Honshu volcanic groups may result from (i) contamination of a MORB-type mantle source by subducted sediments (*15–17*); (ii) intrinsic mantle heterogeneities (*18*); (iii) involvement of old, enriched mantle lithosphere (*19*); or (iv) assimilation of overlying crust (*3, 6*). Stern (*15*) argued that, in the Andes, a change in composition of a continent-derived, subducted sedimentary flux could account for the observed chemical changes along the strike. In Honshu, the strike of the TTL is

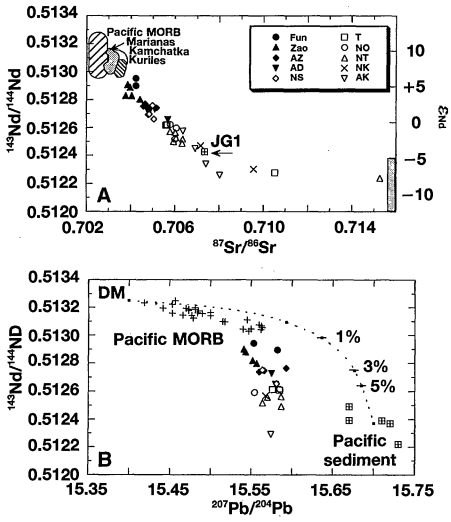

Fig. 4. (**A**) Plot of $^{143}Nd/^{144}Nd$ versus $^{87}Sr/^{86}Sr$ ratios of the Honshu lavas. Data from Pacific MORB (*27*), Cretaceous granite (JG1), (*22*), Marianas (*28*), Kuriles (*30*), and Kamchatka (*29*) are shown for comparison. The shaded box in the lower right represents the present-day range of the lower crust [−5 to −13 $\varepsilon_{Nd}(0)$] south of the TTL. (**B**) Plot of $^{143}Nd/^{144}Nd$ versus $^{207}Pb/^{204}Pb$ ratios, comparing data for the Honshu lavas to data for sediments from DSDP hole 579 and MORB. The dashed curve is a mixing line between depleted mantle (DM) (*31*) and average sediment, with the proportion of sediment indicated by tick marks.

Table 1. Chemical and isotopic data for lavas of Quaternary volcanoes in northern Honshu, Japan (*24*).

Sample number	Amount of (weight %)		$^{206}Pb/^{204}Pb$	$^{207}Pb/^{204}Pb$	$^{208}Pb/^{204}Pb$	$^{87}Sr/^{86}Sr$	$^{143}Nd/^{144}Nd$	ε_{Nd}
	SiO_2	MgO						
Funagata								
Fun a	50.26	5.42	18.42	15.55	38.40	0.70422	0.512945	5.99
Fun b	51.42	5.11	18.48	15.58	38.51	0.70424	0.512894	4.99
Zao								
5Z4	55.13	4.84	18.40	15.54	38.34	0.70397	0.512881	4.74
6Z1	58.41	2.47				0.70375	0.512822	3.59
6Z2	60.65	3.29	18.42	15.56	38.40	0.70440	0.512798	3.12
6Z3	58.17	4.14	18.41	15.55	38.38	0.70403	0.512820	3.55
6Z19	49.57	6.00	18.37	15.54	38.34			
6Z21	49.00	7.36	18.37	15.54	38.32	0.70385	0.512901	5.13
Azuma								
7AZ4	55.30	4.84	18.48	15.59	38.55	0.70464	0.512764	2.46
7AZ9	62.31	3.12	18.45	15.56	38.45	0.70486	0.512737	1.93
7AZ10	58.06	4.31				0.70517	0.512735	1.89
7AZ17	56.73	4.75	18.45	15.57	38.47	0.70457	0.512747	2.13
Adatara								
8AD4	57.90	4.14	18.47	15.57	38.49	0.70508	0.512726	1.72
8AD5	60.54	2.95				0.70490	0.512730	1.79
8AD7	55.83	3.52	18.48	15.58	38.52	0.70567	0.512650	0.23
8AD10	60.14	3.02				0.70473	0.512736	1.91
8AD12	59.18	3.64				0.70474	0.512722	1.64
Nasu								
10NS1	56.24	5.08	18.43	15.58	38.54	0.70503	0.512654	0.31
10NS4	54.56	6.48	18.41	15.56	38.47	0.70498	0.512752	2.22
10NS12	53.60	6.16	18.42	15.58	38.53	0.70449		
10NS23	58.47	3.75				0.70479	0.512686	0.94
11NS1	53.12	4.86				0.70483	0.512689	0.99
Takahara								
11T2	54.42	5.08	18.41	15.58	38.54	0.70565	0.512612	−0.51
11T4	55.03	5.02	18.43	15.59	38.58	0.70559	0.512619	−0.57
11T10	66.49	1.04				0.71052	0.512265	−7.28
Nyoho								
14NO1	62.64	2.14				0.70599	0.512510	−2.50
14NO5	50.86	4.74	18.37	15.55	38.48	0.70605	0.512592	−0.90
14NO10	55.49	3.83	18.41	15.58	38.56	0.70578	0.512615	−0.45
Nantai								
12NT2	65.45	1.53				0.70635	0.512510	−2.50
12NT3	52.72	5.21	18.38	15.57	38.50	0.70601	0.512557	−1.58
12NT5	61.91	2.13	18.43	15.59	38.63			
12NT11	57.66	3.62	18.42	15.59	38.61			
12NT13	56.34	4.07	18.39	15.56	38.54	0.70605	0.512517	−2.36
12NT17	52.74	5.53	18.42	15.59	38.58	0.70594	0.512491	−2.87
12NT20	61.83	2.27				0.70633	0.512478	−3.12
Nantai1	63.99	1.95	18.42	15.59	38.57	0.70577	0.512562	−1.48
Nantai3	73.06	0.07				0.71528	0.512228	−8.00
Nikko Shirani								
13NK4	74.56	0.20				0.70716	0.512461	−3.45
13NK5	74.00	0.29	18.41	15.57	38.63	0.70956	0.512292	−6.75
Akagi								
15AK1	70.62	0.69				0.70691	0.512441	−3.84
15AK4	57.70	3.31				0.70739	0.512330	−6.01
16AK1	59.72	3.15				0.70803	0.512251	−7.55
16AK4	53.72	3.75	18.41	15.57	38.48	0.70635	0.512568	−1.37
16AK7	56.63	3.85				0.70735		

oblique to the trench (Fig. 1), making it unlikely that isotopically distinct, subducted sediment derived from the continent could be selectively and coincidentally isolated at depth to either side of the TTL.

Oceanic sediments recovered from Deep Sea Drilling Project (DSDP) site 579 east of the Japan trench (Fig. 1) have approximately the same bulk composition as sediment now being subducted beneath Honshu (*20*); thus, these sediments represent the best analog for sediments subducted earlier. If the Pb isotopic compositions from this one sediment core (Fig. 3C) are representative, it is doubtful that an average subducted sediment composition could account for the fine Pb isotopic distinctions present in the arc lavas. The Nd and Pb data further demonstrate that the distinctive isotopic ratios of the Honshu lavas are not the result of mixing between a depleted mantle source and sediment (Fig. 4B). A mixing curve between the two likely end-members does not pass through either of the Honshu lava groups. This simple mixing calculation shows that sediments near the Japan trench do not have the appropriate isotopic composition to produce the distinct signatures of the Honshu lavas.

If an age significance can be attached to the Pb isotope arrays (Fig. 3B), calculated $^{207}Pb/^{206}Pb$ ages for the northern and southern volcanoes are 3.8×10^9 and 4.0×10^9 years, respectively. These ages are quite old and are unlikely to correspond to the timing of a mantle-melting event, as the effects of mantle convection would prevent long-term isolation of distinct isotopic domains. More likely, these linear trends are mixing lines without age significance, and isotopic variations in the lavas do not reflect heterogeneity in the asthenospheric portion of the mantle. Incorporation of radiogenic Pb in the Honshu suites from isolated, nonconvecting lithospheric mantle is possible, although O isotopic compositions of basalts from volcanoes of the Honshu transect ($\delta^{18}O$ ranging from +6.2 to +7.4 per mil) are significantly heavier compared to normal mantle values ($+5.7 \pm 0.3$ per mil) (*21*). These data imply that the composition of the rocks reflects crustal contamination rather than involvement of old lithospheric mantle.

The Honshu data can best be explained in terms of mixing between basalts derived from a fluid-fluxed mantle wedge and isotopically distinct crustal components characterized by high $^{208}Pb/^{204}Pb$, $^{207}Pb/^{204}Pb$, and $^{87}Sr/^{86}Sr$ ratios and low $^{143}Nd/^{144}Nd$ ratios. Basalt is emplaced into the lower crust where open-system, crust-magma interaction includes assimilation of old continental material, fractional crystallization, and recharge (*3*, *5*, *6*). Differential degrees of mixing between depleted mantle, old crust, and hybrid magmas may account for the large variation preserved within individual volcanic centers. The radiogenic and stable isotopic data clearly indicate that all the lavas, even those with >5% by weight MgO, have been contaminated with crustal material.

The Nd model ages of exposed crustal granites can be used to place limits on the isotopic composition of the unexposed lower crust. The ε_{Nd} (see Table 1) (-3.7 at 90×10^6 years) of JG1, a representative Cretaceous granodiorite located between Akagi and Nikko volcanoes (Fig. 4A), is consistent with the production by mixing of mantle- and lower crustal–derived components (*22*). The Sm-Nd model age of JG1 [depleted mantle model age (T_{DM}) $\sim 1.25 \times 10^9$ years] provides a minimum age for the lower crustal contaminant that is significantly older than any crustal materials exposed south of the TTL. On the basis of this model age, we estimate an upper limit on the present-day range of initial $\varepsilon_{Nd}(0)$ of -5 to -13 for the lower crust of Honshu south of the TTL, depending on whether it was derived from a chrondritic or depleted mantle reservoir (Fig. 4A). A lower crust of this isotopic character could represent an end-member reservoir for all the lavas erupted south of the TTL. The upper crust, as represented by granodioritic composition JG1, is not a possible end-member reservoir. These ages are in the same range as Sm-Nd model ages (T_{DM}) for Precambrian basement rocks in Korea (*23*), equivalents of which may underlie older terranes of western and central Honshu (*11*). The composition of the lower crust north of the TTL is less well constrained. The least radiogenic volcanic samples have a T_{DM} of $\sim 270 \times 10^6$ years, providing a minimum age for the crustal contaminant of the lavas north of the TTL. This age is significantly older than that of any exposed Abukuma terrane rocks. The high Pb isotope ratios of the volcanoes north of the TTL are also consistent with the involvement of Precambrian lower crust in magmagenesis.

The Honshu data provide evidence that mixing of mantle-derived basalts with lower crustal reservoirs is an important process in island arc volcanism. As a result of the fortuitous tectonic situation in the overriding plate, the crustal portion of the lithosphere plays an important role in modifying the composition of mantle-derived melts. In northern Honshu, two juxtaposed isotopically distinct lower crustal reservoirs have sufficient isotopic leverage for their contributions to be discernible, but this effect may be difficult to demonstrate in arcs where the crust is younger. Recognizing that the Pb, Sr, and Nd isotopic ratios in these arc lavas appear to be derived from overriding lithospheric sources, we believe that attributing similarly high ratios in other arcs solely to a subducted sediment contribution would be unwise.

REFERENCES AND NOTES

1. D. J. DePaolo, F. V. Perry, W. S. Baldridge, *Trans. R. Soc. Edinburgh Earth Sci.* **83**, 439 (1992).
2. J. B. Gill, *Orogenic Andesites and Plate Tectonics* (Springer-Verlag, New York, 1981); Y. Tatsumi, *J. Geophys. Res.* **94**, 4697 (1989).
3. W. Hildreth and S. Moorbath, *Contrib. Mineral. Petrol.* **98**, 455 (1988).
4. J. P. Davidson *et al.*, *ibid.* **105**, 412 (1990).
5. C. H. Chen, D. J. DePaolo, S. Nakada, Y. N. Shieh, *Nature* **362**, 831 (1993).
6. G. Worner *et al.*, *Large- and Fine-Scale Geochemical Variations Along the Andean Arc of Northern Chile (17.5–22S)* (Springer-Verlag, Berlin, 1992).
7. R. D. Jarrard, *Rev. Geophys.* **24**, 217 (1986).
8. N. Nasu *et al.*, *Init. Rep. Deep Sea Drill. Program* **56–57 (part 2)**, 408 (1980).
9. D. Zhao, A. Hasegawa, H. Kanamori, *J. Geophys. Res.* **99**, 22313 (1994).
10. T. Plank and C. H. Langmuir, *Earth Planet. Sci. Lett.* **90**, 349 (1988). Plank and Langmuir argued that the thickness of crustal lithosphere in the overlying arc controls the degree of melting and that increases in crustal thickness are inversely correlated with melting.
11. S. Mizutani, in *Pre-Cretaceous Terranes of Japan*, K. Ichikawa, S. Mizutani, I. Hara, S. Hada, A. Yao, Eds. (Nippon Insatsu Shuppan Co. Ltd., Osaka, 1990), pp. 121–136.
12. L. Jolivet and K. Tamaki, *Proc. Ocean Drilling Program, Sci. Results* **127–128 (part 2)**, 1311 (1992).
13. M. Faure and B. Natal'in, *Tectonophysics* **208**, 397 (1992).
14. K. Notsu, *J. Volcanol. Geotherm. Res.* **18**, 531 (1983); K. Sato, S. Ishihara, K. Shibata, *Geol. Atlas Jpn. Sheet* **7** (1992).
15. C. R. Stern, *Geology* **19**, 78 (1991).
16. R. W. Kay, S. S. Sun, C. N. Lee-Hu, *Geochim. Cosmochim. Acta* **42**, 263 (1978).
17. J. D. Morris, W. P. Leeman, F. Tera, *Nature* **344**, 31 (1990).
18. J. Barling and S. L. Goldstein, *ibid.* **348**, 59 (1990).
19. G. Rogers and C. J. Hawkesworth, *Earth Planet. Sci. Lett.* **91**, 271 (1989).
20. B. L. Cousens, J. F. Allan, M. P. Gorton, *Contrib. Mineral. Petrol.* **117**, 421 (1994).
21. Y. Matsuhisa, *J. Volcanol. Geotherm. Res.* **5**, 271 (1979); K. Muehlenbachs and R. N. Clayton, *Can. J. Earth Sci.* **9**, 172 (1972). The quantity $\delta^{18}O$ is defined as:

$$\delta^{18}O = \left[\frac{(^{18}O/^{16}O)_{sample}}{(^{18}O/^{16}O)_{standard}} - 1\right] \times 10^3$$

22. S. Nohda and G. J. Wasserburg, *Earth Planet. Sci. Lett.* **52**, 264 (1981).
23. C.-Y. Lan, T. Lee, X.-H. Zhou, S.-T. Kwon, *Geology* **23**, 249 (1995).
24. The Pb isotope ratios are corrected for mass fractionation by 0.84 per mil per atomic mass unit on the basis of multiple analyses of National Bureau of Standards standard 981. Analytical uncertainties (2σ) are estimated at $^{206}Pb/^{204}Pb = 0.012$, $^{207}Pb/^{204}Pb = 0.017$, and $^{208}Pb/^{204}Pb = 0.055$. We duplicated 10% of the samples for Pb. All duplicates fell within analytical error. The $^{87}Sr/^{86}Sr$ values are normalized to $^{86}Sr/^{88}Sr = 0.1194$ to correct for mass discrimination; estimated analytical uncertainty is ± 0.00001 (2σ). The ε_{Nd} values represent $^{143}Nd/^{144}Nd$ ratios normalized to a standard chondritic value: $\varepsilon_{Nd} = (^{143}Nd/^{144}Nd_{measured}/^{143}Nd/^{144}Nd_{chrondritic} - 1) \times 10^4$; $^{143}Nd/^{144}Nd_{chrondritic}$ is 0.512638, and we did the correction for mass discrimination assuming $^{146}Nd/^{144}Nd = 0.7219$; estimated analytical uncertainty is ± 0.00002 (2σ).
25. K. Ichikawa, in *Pre-Cretaceous Terranes of Japan*, K. Ichikawa, S. Mizutani, I. Hara, S. Hada, A. Yao, Eds. (Nippon Insatsu Shuppan, Osaka, 1990), pp. 1–11.
26. L. Jolivet, J. P. Cadet, F. Lalevee, *Tectonophysics* **149**, 89 (1988).
27. W. M. White, A. W. Hofmann, H. Puchelt, *J. Geophys. Res.* **92**, 4881 (1987).
28. J. D. Woodhead and D. G. Fraser, *Geochim. Cosmochim. Acta* **49**, 1925 (1985).
29. A. B. Kersting and R. J. Arculus, *Earth Planet. Sci. Lett.* **136**, 133 (1995).

30. J. C. Bailey, O. Larsen, T. I. Frolova, *Contrib. Mineral. Petrol.* **95**, 155 (1987).
31. A. Zindler and S. R. Hart, *Annu. Rev. Earth Planet. Sci.* **14**, 493 (1986).
32. A.B.K. extends appreciation to J. B. Rundle, F. J. Ryerson, and G. Zandt for support. Logistical and field support from I. Kushiro and K. Kaneko is gratefully acknowledged. Reviews by K. Mezger, C. R. Stern, and two anonymous reviewers improved the manuscript. This work was funded by the Institute of Geophysics and Planetary Physics under the auspices of Department of Energy contract W-7405-Eng-48 and the Australian Research Council. This is publication 56 of the GEMOC Key Centre for teaching and research.

29 January 1996; accepted 18 April 1996

Amorphization of Serpentine at High Pressure and High Temperature

Tetsuo Irifune,* Koji Kuroda, Nobumasa Funamori, Takeyuki Uchida, Takehiko Yagi, Toru Inoue, Nobuyoshi Miyajima

Pressure-induced amorphization of serpentine was observed at temperatures of 200° to 300°C and pressures of 14 to 27 gigapascals with a combination of a multianvil apparatus and synchrotron radiation. High-pressure phases then crystallized rapidly when the temperature was increased to 400°C. These results suggest that amorphization of serpentine is an unlikely mechanism for generating deep-focus earthquakes, as the temperatures of subducting slabs are significantly higher than those of the rapid crystallization regime.

The occurrence of deep-focus earthquakes at depths of 100 to 670 km in the mantle has been a puzzle because the brittle fracture should be prohibited under the pressure and temperature conditions corresponding to these depths. A number of mechanisms have been proposed for the deep-focus earthquakes (*1*, *2*), but each has certain weaknesses. One proposed mechanism is pressure-induced dehydration and amorphization of serpentine, a major hydrous phase in the subducting oceanic lithosphere (*3*). Acoustic emissions have been associated with either the dehydration or amorphization of serpentine at pressures of up to 25 GPa in a diamond anvil cell (*2*). However, the direct observations of pressure-induced amorphization of serpentine were made at room temperature only. It has thus remained unclear whether the acoustic emissions observed between 6 and 25 GPa at temperatures of up to about 600°C (*2*) were actually related to the amorphization of serpentine. We therefore examined the temperature and pressure conditions for the amorphization of serpentine using in situ synchrotron radiation x-ray diffraction measurements and a double-stage multianvil high-pressure apparatus.

We used natural antigorite with a composition of $(Mg_{0.95}, Fe_{0.05})_3Si_2O_5(OH)_4$ as the starting material. We also used a natural lizardite to study the effect of the crystallographic form on amorphization. The powdered sample was mixed with a Au powder for pressure measurements (*4*) and enclosed in a capsule made of cemented amorphous boron. Twin-sheet heaters of TiC were used, and the temperature was monitored with a $W_{97}Re_3$-$W_{26}Re_{74}$ thermocouple (*5*). In situ x-ray diffraction measurements at high pressures and high temperatures were performed at the National Laboratory for High Energy Physics (KEK) with a hybrid anvil system (*6*).

We carried out four runs at pressures up to 28 GPa and at temperatures up to 1500°C (Fig. 1). For the first run (ME-1), containing antigorite, the pressure was increased slowly to 27 GPa at room temperature over 14 hours. The x-ray pattern was taken for 5 to 10 min after the pressure was held for 10 to 30 min every 2 to 3 GPa. Virtually no changes were observed in the diffraction patterns at pressures up to 27 GPa (Fig. 2, A and B); thus, no amorphization of antigorite was observed with compression at room temperature.

Next, the temperature of the sample was gradually increased to 1200°C over 6 hours at 27 GPa. Diffraction patterns were collected after every 50° to 100°C increase, and we monitored the pressure change at the fixed press load during the heating (*7*). The intensities of the diffraction peaks of antigorite decreased compared with those of Au at temperatures near 200°C, and the peaks disappeared at this temperature in a few minutes (Fig. 2C). A diffraction halo, characteristic of an amorphous material, appeared as the diffraction peaks disappeared; thus, antigorite was converted to an amorphous state at these temperatures within 10 min. With further heating, a few new diffraction peaks appeared at temperatures near 400°C, and these grew rapidly (Fig. 2, D and E). X-ray diffraction and electron microprobe data for the sample quenched from 1200°C at 24 GPa show the presence of phase D (*8*) and superhydrous B. Similar results were obtained with lizardite (run ME-3) at pressures of about 26 GPa (Fig. 1).

We also obtained similar results near 19 GPa (run ME-2, Fig. 3), except that amorphization of serpentine started at slightly higher temperatures (by ~ 50°C) (Fig. 1). The final products of this run, at 20 GPa and 1050°C, were γ-$(Mg, Fe)_2SiO_4$ + stishovite (+ water).

In contrast, at pressures of 10 to 13 GPa, we did not observe any clear evidence of amorphization of antigorite either at room temperature or at high temperatures (run ME-6, Fig. 1). Although the intensity of some diffraction peaks decreased slightly relative to those of Au at 400°C, high-pressure phases crystallized rapidly above 450°C. The quenched product from 1200°C at 11 GPa consisted of α-$(Mg, Fe)_2SiO_4$ + clinoenstatite (+ water).

Thus, in all of our runs, serpentine did not become amorphous over 14 to 30 hours

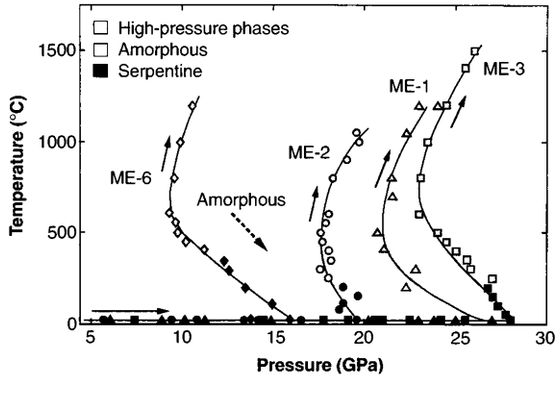

Fig. 1. The temperature and pressure conditions of in situ x-ray diffraction measurements and summary of the experimental runs to examine the amorphization of serpentine. Antigorite (ME-1, ME-2, and ME-6) and lizardite (ME-3) were used as starting materials. The "amorphous" region denotes the conditions where amorphization of serpentine was observed while no high-pressure phases were encountered.

T. Irifune and K. Kuroda, Department of Earth Sciences, Ehime University, Matsuyama 790, Japan.
N. Funamori, T. Uchida, T. Yagi, Institute for Solid State Physics, University of Tokyo, Roppongi, Minato-ku 106, Japan.
T. Inoue, Center for High Pressure Research, State University of New York, Stony Brook, NY 11794, USA.
N. Miyajima, Department of Earth and Planetary Sciences, Hokkaido University, Sapporo 060, Japan.
*To whom correspondence should be addressed.